Spatially-Resolved Structure and Electronic Properties of Graphene on Polycrystalline Ni

Jiebing Sun,[†] James B. Hannon,[‡,*] Rudolf M. Tromp,[‡] Priya Johari,[§] Ageeth A. Bol,[‡] Vivek B. Shenoy,[§] and Karsten Pohl[†]

[†]Physics Department and Materials Science Program, University of New Hampshire, Durham, New Hampshire 03824, United States, [‡]IBM Research Division, T.J. Watson Research Center, Yorktown Heights, New York 10598, United States, and [§]Division of Engineering, Brown University, Providence, Rhode Island 02912, United States

ABSTRACT We have used *in situ* low-energy electron microscopy (LEEM) to correlate the atomic and electronic structure of graphene films on polycrystalline Ni with nm-scale spatial resolution. Spatially resolved electron scattering measurements show that graphene monolayers formed by carbon segregation do not support the π-plasmon of graphene, indicating strong covalent bonding to the Ni. Graphene bilayers have the Bernal stacking characteristic of graphite and show the expected plasmon loss at 6.5 eV. The experimental results, in agreement with first-principles calculations, show that the π-band structure of free-standing graphene appears only in films with a thickness of at least two layers and demonstrate the sensitivity of the plasmon loss to the electronic structure.

KEYWORDS: graphene CVD growth · graphene structure · plasmons · LEEM

The deposition of carbon onto metal foils and thin films is currently the leading method for producing large, continuous graphene films.[1,2] One of the earliest approaches involves segregating carbon from the saturated bulk of a Ni thin film.[3] The segregated carbon forms graphene, with a layer thickness that depends on the amount of segregated carbon. Owing to the complexity of polycrystalline films, graphene formation *via* segregation is an extremely difficult process to understand and control. Interface heterogeneity also complicates efforts to quantitatively predict graphene device performance, for example, charge transport through graphene/metal contacts.[4,5] Unambiguous characterization of graphene on heterogeneous surfaces necessarily requires a local probe of both atomic *and* electronic structure.

Here we describe a combined measurement of the atomic and electronic structure of graphene films with 10 nm lateral spatial resolution. As we subsequently show, monolayer graphene is strongly bound to the Ni surface and does not support the expected π-bands of free-standing graphene, which appear only after two layers have formed. Our results are consistent with first-principles electronic structure calculations for monolayer and bilayer graphene films on Ni(111). We show that the graphene π-plasmon is a sensitive probe of the graphene band structure near the Fermi level. By forming images using electrons that excite graphene plasmons, we directly correlate local electronic properties with local surface structure.

RESULTS AND DISCUSSION

After preparation of a clean surface, Ni(111) grains of 1−2 μm in diameter are observed. A low-energy electron microscopy (LEEM)[6] image of the clean polycrystalline Ni(111) surface, along with the corresponding electron diffraction pattern, is shown in Figure 1a. Graphene films of varying thickness were formed by segregation of carbon to the surface at 800 °C. When the desired amount of carbon had segregated, the process was halted by rapidly cooling the substrate to room temperature. A LEEM image after carbon segregation and graphene formation is shown in Figure 1b. As we show later, the darker regions in the image correspond to monolayer graphene, while the brighter areas, located near the grain boundaries, are thicker (2−3 layers).

Because the surface is polycrystalline and rough, conventional LEED is of limited usefulness. The beam samples a large area of the surface, encompassing hundreds of randomly oriented and misaligned grains, resulting in a diffraction pattern that is complex and difficult to interpret, as shown in the inset to Figure 1a. However, by

*Address correspondence to jbhannon@us.ibm.com.

Received for review August 26, 2010 and accepted October 29, 2010.

Published online November 9, 2010.
10.1021/nn102167f

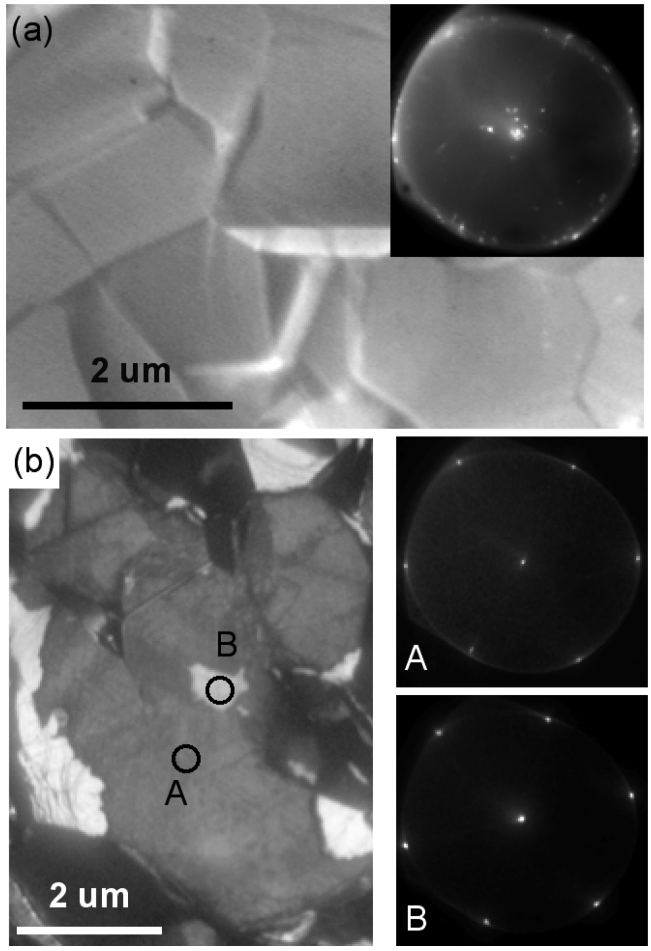

Figure 1. (a) A 10 eV bright-field LEEM image of a polycrystalline Ni(111) surface. The inset shows the electron diffraction pattern (68 eV) from a 10 μm diameter area; (b) 10 eV bright-field LEEM image recorded after graphene segregation. At this electron energy, one graphene layer (A) appears dark, while thicker areas (B) are bright. Selected area electron diffraction patterns (68 eV) from the areas marked A and B in panel b.

illuminating only small regions of the surface (~500 nm diameter), diffraction patterns from selected areas of *individual grains* can be easily obtained (Figure 1b). Almost exclusively we observe a 1 × 1 diffraction pattern, indicating that the graphene is azimuthally locked to the underlying Ni(111) lattice. Because the graphene film is commensurate with the substrate, it is difficult to detect the presence of graphene from the electron diffraction pattern alone. Instead, we confirmed the presence of graphene by analyzing the dependence of the image intensity on the electron energy, in the spirit of a "LEED-IV" measurement.[7]

The dependence of the diffracted intensity on the electron energy is known as an "IV curve". The structure of the surface can be determined with subangstrom precision by comparing the measured IV curves with those computed for a trial structure.[8] In LEEM, the IV curve for any pixel in the image (10 × 10 nm^2) can be extracted from a series of images recorded as the incident electron energy is changed.[7] IV curves measured on a clean Ni(111) grain, and from the regions marked A and B in Figure 1b, are shown in Figure 2. It is clear that the segregation of carbon causes a dramatic change in the IV curve, and that the curves from the regions marked A and B are qualitatively different.

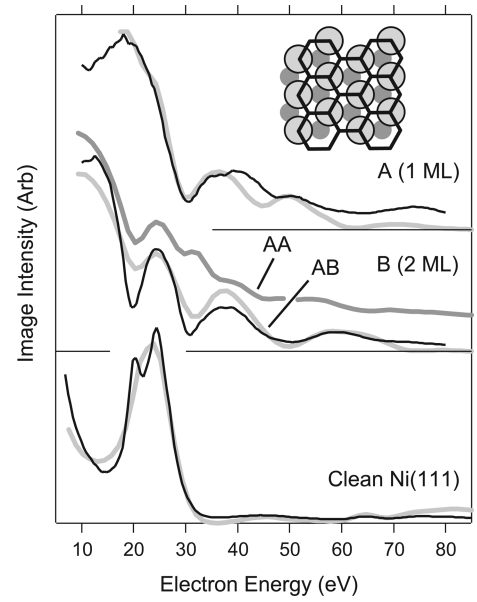

Figure 2. Measured (black) and computed (gray) diffraction curves (image intensity) from a clean Ni(111) grain and from the regions A and B in Figure 1b. The best-fit curve for a graphene bilayer with AA stacking is shown in dark gray. The inset shows the measured registry of one graphene layer on Ni(111). First-layer Ni atoms are light gray and second-layer atoms are dark gray.

Dynamical analyses of the IV curves were performed using codes based on the LEEDOpt package.[9] Eight phase shifts ($L = 7$) were used for the atomic *t*-matrix calculation at each energy. An energy-dependent optical potential of the form $0.85E^{1/3}$ was assumed.[10] Trial surface structures were optimized to minimize the R_2 factor.[9] For clean Ni(111) the best fit corresponds to a bulk terminated (111) surface. For region A the best fit corresponds to one monolayer of graphene located 2.18 Å above the Ni(111) surface. The graphene layer has the lateral registry indicated in the inset to Figure 2. The hexagons of the graphene lattice are centered on the Ni atoms in the *second* layer. This result is in quantitative agreement with the previous LEED analysis of Gamo *et al.* for single-crystal Ni(111).[11]

The IV curve from region B is significantly different from that of A. For this region, the best-fit corresponds to two graphene layers with the AB (Bernal) stacking sequence found in graphite. The derived layer spacing of 3.33 Å compares well with the value of 3.35 Å found in graphite. It is clear from Figure 2 that AA stacking gives a considerably worse fit than AB stacking. A random orientation of the graphene is ruled out by the 1 × 1 diffraction pattern (Figure 1b).

The LEEM instrument used in these experiments is equipped with an in-line electron energy filter,[12] enabling spatially resolved electron-energy loss spectroscopy (EELS) measurements. A convenient method of

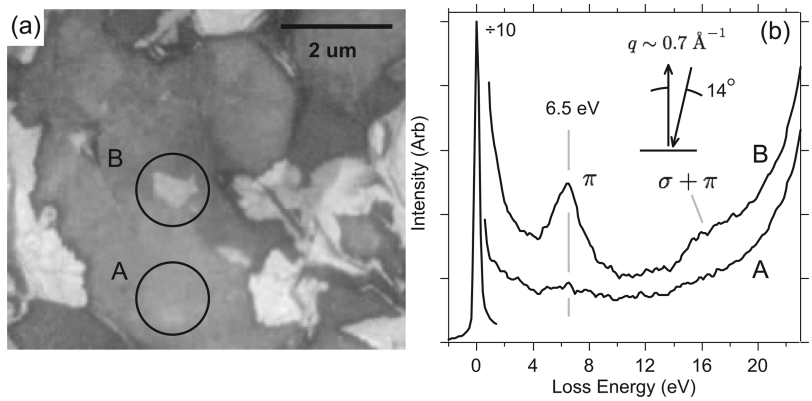

Figure 3. (a) Energy-filtered LEEM image. The image is formed from electrons that have lost energy in the range 4−7 eV, *i.e.,* from those electrons that have excited a graphene π plasmon at the surface. The incident electron energy was 33 eV. (b) Electron energy loss spectra (33 eV incident energy) recorded from the areas labeled A and B in panel A. Region A has a single graphene monolayer and the EELS spectrum shows no π-plasmon loss feature. Region B corresponds to two graphene layers and shows the expected π-plasmon loss at 6.5 eV and σ + π plasmon loss at 16 eV.

probing the electronic structure of the graphene layer is to measure the excitation of surface plasmons.[13−20] As we show below, it is possible to perform plasmon spectroscopy with 10 nm spatial resolution, allowing a direct correlation of the local atomic and electronic structure. The collective excitation of the π electrons in graphene gives rise to a characteristic loss feature in the 6−8 eV range.[21] Using first-principles electronic structure calculations, we show that the presence of this feature in the loss spectrum indicates the presence of the graphene π-band structure.

An energy-filtered LEEM image of the same region shown in Figure 1b is shown in Figure 3a. The incident electron energy was 33 eV. The image was formed from reflected electrons that have lost energy in the range of 4−7 eV. Incident electrons that excite the π-plasmon of graphene will fall in this energy window, and the bright areas in Figure 3a indicate where plasmons are excited in the surface. It is clear that the bright areas in this "plasmon image" correspond precisely to the thicker graphene areas in Figure 1b.

An even clearer picture develops when spatially resolved EELS spectra are recorded from the monolayer and bilayer regions of the surface. We do this by illuminating 1.5 μm diameter areas of the surface (indicated by the circles in Figure 3a) and energy-analyzing the reflected electrons. The results are shown in Figure 3b. Spectrum B was recorded from a region that includes bilayer graphene (as indicated in figure 3a). This spectrum shows a clear loss feature at 6.5 eV, which corresponds to the π-plasmon of graphene.[15,18−20] A weaker feature at 16 eV corresponds to the σ + π plasmon. Spectrum A was recorded from monolayer graphene. There are no loss features in the spectrum, suggesting that the band structure of graphene is absent, despite the fact that a carbon layer with the graphene structure is present.

To establish the link between the appearance of the π-plasmon and the band structure of graphene, we performed first-principles density functional theory (DFT) calculations using the *ab initio* simulation package VASP.[22,23] Projector-augmented wave (PAW)[24,25] potentials were used to represent the ionic cores. Exchange and correlation effects were treated in the generalized gradient approximation (GGA) proposed by Perdew, Burke, and Ernzerhof.[26] The structures of monolayer and bilayer graphene on Ni(111) were modeled using a supercell with six layers of Ni and a vacuum region of 12 Å. The bottom three Ni(111) layers were kept fixed at the optimized bulk Ni−Ni bond distance, $d = 2.038$ Å, while the top three Ni layers, along with the graphene layers, were allowed to relax. A planewave cutoff of 400 eV and a $43 \times 43 \times 1$ *k*-point sampling was used. The distance between Ni and the first graphene layer was found to be 2.13 Å, which is in excellent agreement with the value derived from the LEED analysis. In the case of bilayer graphene, the Ni−C distance was found to be the same as in the case of single layer graphene, but the interlayer spacing of 3.83 Å obtained between the graphene layers is about 15% larger than the experimental value.

The EELS loss function was computed by taking the imaginary part of the inverse of the in-plane (*xx* or *yy*; note that the normal to the graphene layers is along the *z* -axis) component of the dielectric constant tensor, $\varepsilon_{\alpha\beta}$, in the random phase approximation (RPA).[27] The imaginary part of the dielectric constant tensor is given as

$$\varepsilon^{(2)}_{\alpha\beta}(\omega) = \frac{4\pi^2 e^2}{\Omega} \lim_{q\to 0} \frac{1}{q^2} \sum_{c,v,\mathbf{k}} 2w_{\mathbf{k}} \delta(\varepsilon_{c\mathbf{k}} - \varepsilon_{v\mathbf{k}} - \omega) \langle u_{c\mathbf{k}+e_\alpha q} | u_{v\mathbf{k}} \rangle \langle u_{c\mathbf{k}+e_\beta q} | u_{v\mathbf{k}} \rangle^* \quad (1)$$

Here the indices *c* and *v* refer to the conduction and the valence band states, respectively, $u_{\mathbf{k}}$ is an eigenstate with wave vector **k**, $w_{\mathbf{k}}$ are the *k*-point weights, which are defined such that they sum to 1,[28] the factor 2 before the weights accounts for the fact that a spin-degenerate system is considered, and Ω is the volume

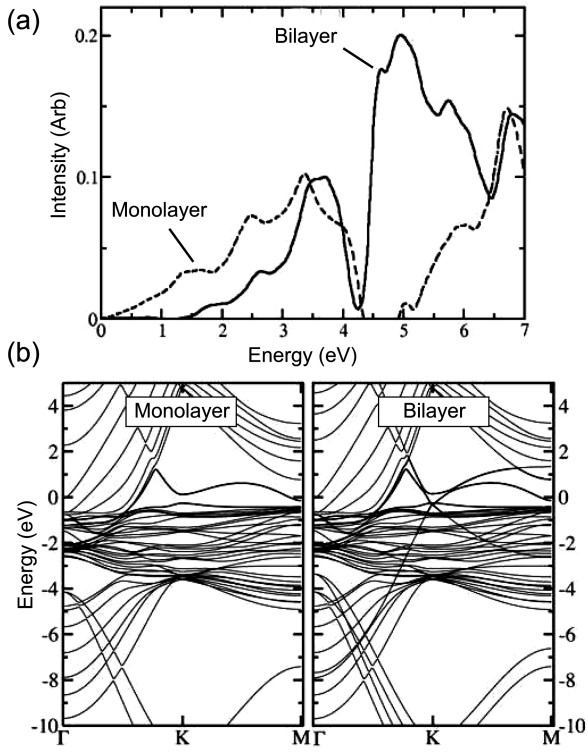

Figure 4. (a) The calculated loss spectra of monolayer and bilayer graphene on Ni(111) for $q \approx 0$. A line width of 0.01 eV was used to compute the spectra. (b) Band structure of monolayer and bilayer graphene on Ni(111). The Dirac point is clearly observed at *K* in the case of bilayer graphene but not for monolayer graphene.

of the unit cell. The vectors e_α are the unit vectors for the three Cartesian directions. It is known from the work of Eberlein *et al.*[15] that in graphene, the π and $\pi + \sigma$ plasmon peaks appear at around 4.8 and 15 eV, respectively for $q \approx 0$. For both free-standing monolayer and bilayer graphene we have obtained spectra essentially identical to those computed by Eberlein *et al.*,[15] thus confirming the validity of our approach (more sophisticated approaches to computing the dielectric function can be found elsewhere[16,17]). To examine the π-plasmon features on Ni(111), we computed the loss spectra for both monolayer and bilayer graphene in the range 0−7 eV (Figure 4). For the case of monolayer graphene, there is no loss peak corresponding to the π -plasmon excitation (dashed line in Figure 4a). However, for bilayer graphene (solid line), there is a clear feature at the expected loss energy of 4.8 eV. The position of the calculated π plasmon, however, is slightly red-shifted when compared to the measured spectra. This can be understood by noting that the calculated spectra are for $q = 0$, while the measured spectra correspond to $q = 0.7$ Å $^{-1}$. Away from $q = 0$, the π-plasmon shows a clear dispersion to higher energies, consistent with what we observe.[13,14,18] Thus, we conclude that covalent bonding between graphene and the Ni substrate disrupts the π bands, and that the π bands of graphene only appear when two layers of graphene are present. This is also evident from the band structures of graphene and bilayer graphene on Ni(111) shown in Figure 4; the Dirac point is only present in the case of bilayer graphene, while for monolayer graphene there are no crossing graphene bands near the *K*-point.

CONCLUSION

We have used electron diffraction and spectroscopy, with nanometer-scale spatial resolution, to characterize the geometric and electronic structure of graphene films on a polycrystalline Ni substrate. Single layers of graphene are rotationally locked to the Ni grain on which they reside. The layers are strongly bound to the substrate, and the π-band structure characteristic of graphene is absent. In contrast, graphene bilayers do exhibit the π-plasmon, demonstrating that at least two layers of graphene are required in order for the π-band structure of graphene to appear. The disruption of the graphene band structure at the interface with Ni highlights a potential issue for metal contacts in graphene devices. Clearly, it is not just the metal work function that determines the transport properties of the interface. Bonding of the graphene to the metal can significantly alter the graphene band structure, potentially affecting charge injection and device performance. These results highlight the need for combined measurements of atomic and electronic structure in understanding the properties of graphene films.

METHODS

Sample Fabrication. The polycrystalline Ni films were created by sputter depositing 300 nm of Ni onto 300 nm SiO_2 /Si substrates. The Ni films were cleaned in ultrahigh vacuum (UHV) by sputtering with 2 kV Ne ions at 800 °C, followed by annealing at 900 °C. Surface cleanliness was monitored using X-ray photoelectron spectroscopy (XPS). Annealing at 900 °C produced Ni(111) grains with an average diameter of 1−2 μm.

Graphene Formation. Carbon was dissolved into the Ni film by exposure to 5×10^{-7} Torr of ethylene at 975 °C for about 5 min. After ethylene exposure, segregated graphene layers were formed by gradually lowering the substrate temperature in UHV. Segregation typically occurred at temperatures below 900 °C. All process steps—annealing, ethylene exposure, and carbon segregation—were monitored in real time using LEEM.

Microscopy. The surfaces were imaged using a low-energy electron microscope designed and built at IBM. The microscope incorporates a cold field-emitter electron source and a slit-based energy filter. The microscope is not aberration corrected. Microscopes based on this design are commercially available from SPECS GmbH.

Acknowledgment. This work was supported by DARPA under contract FA8650-08-C-7838 through the CERA program. V.B.S. acknowledges partial support from SRC/NRI and NSF through Grants CMMI-0825771 and CMMI-0855853.

REFERENCES AND NOTES

1. Wintterlin, J.; Bocquet, M.-L. Graphene on Metal Surfaces. *Surf. Sci.* **2009**, *603*, 1841–1852.
2. Li, X.; Cai, W.; An, J.; Kim, S.; Nah, J.; Yang, D.; Piner, R.;

Velamakanni, A.; Jung, I.; Tutuc, E.; *et al.* Large-Area Synthesis of High-Quality and Uniform Graphene Films on Copper Foils. *Science* **2009**, *324*, 1171245.
3. Hayes, A.; Chipman, J. Mechanism of Solidification and Segregation in a Low Carbon. *J. Trans. AIME* **1939**, *135*, 85.
4. Pi, K.; McCreary, K. M.; Bao, W.; Han, W.; Chiang, Y. F.; Li, Y.; Tsai, S.-W.; Lau, C. N.; Kawakami, R. K. Electronic Doping and Scattering by Transition Metals on Graphene. *Phys. Rev. B* **2009**, *80*, 075406.
5. Venugopal, A.; Colombo, L.; Vogel, E. M. Contact Resistance in Few and Multilayer Graphene Devices. *Appl. Phys. Lett.* **2010**, *96*, 013512.
6. Bauer, E. Low-Energy Electron Microscopy. *Rep. Prog. Phys.* **1994**, *57*, 895–938.
7. Sun, J.; Hannon, J. B.; Kellogg, G. L.; Pohl, K. Local Structural and Compositional Determination *via* Electron Scattering: Heterogeneous Cu(001)−Pd Surface Alloy. *Phys. Rev. B* **2007**, *76*, 205414.
8. Pendry, J. B. *Low Energy Electron Diffraction*; Academic Press: London, 1974.
9. Adams, D. L. A Simple and Effective Procedure for the Refinement of Surface Structure in LEED. *Surf. Sci.* **2002**, *519*, 157–172.
10. Demuth, J. E.; Marcus, P. M.; Jepsen, D. W. Analysis of Low-Energy-Electron-Diffraction Intensity Spectra for (001), (110), and (111) Nickel. *Phys. Rev. B* **1975**, *11*, 1460–1474.
11. Gamo, Y.; Nagashima, A.; Wakabayashi, M.; Terai, M.; Oshima, C. Atomic Structure of Monolayer Graphite Formed on Ni(111). *Surf. Sci.* **1997**, *374*, 61–64.
12. Tromp, R. M.; Fujikawa, Y.; Hannon, J. B.; Ellis, A. W.; Berghaus, A.; Schaff, O. A Simple Energy Filter for Low Energy Electron Microscopy/Photoelectron Emission Microscopy Instruments. *J. Phys.: Condens. Matter* **2009**, *21*, 314007.
13. Lin, M. F.; Huang, C. S.; Chuu, D. S. Plasmons in Graphite and Stage-1 Graphite Intercalation Compounds. *Phys. Rev. B* **1997**, *55*, 13961–13971.
14. Pichler, T.; Knupfer, M.; Golden, M. S.; Fink, J.; Rinzler, A.; Smalley, R. E. Localized and Delocalized Electronic States in Single-Wall Carbon Nanotubes. *Phys. Rev. Lett.* **1998**, *80*, 4729–4732.
15. Eberlein, T.; Bangert, U.; Nair, R. R.; Jones, R.; Gass, M.; Bleloch, A. L.; Novoselov, K. S.; Geim, A.; Briddon, P. R. Plasmon Spectroscopy of Free-Standing Graphene Films. *Phys. Rev. B* **2008**, *77*, 233406.
16. Kramberger, C.; Hambach, R.; Giorgetti, C.; Rümmeli, M. H.; Knupfer, M.; Fink, J.; Büchner, B.; Reining, L.; Einarsson, E.; Maruyama, S.; *et al.* Linear Plasmon Dispersion in Single-Wall Carbon Nanotubes and the Collective Excitation Spectrum of Graphene. *Phys. Rev. Lett.* **2008**, *100*, 196803.
17. Trevisanutto, P. E.; Giorgetti, C.; Reining, L.; Ladisa, M.; Olevano, V. *Ab Initio GW* Many-Body Effects in Graphene. *Phys. Rev. Lett.* **2008**, *101*, 226405.
18. Lu, J.; Loh, K. P.; Huang, H.; Chen, W.; Wee, A. T. S. Plasmon Dispersion on Epitaxial Graphene Studied Using High-Resolution Electron Energy-Loss Spectroscopy. *Phys. Rev. B* **2009**, *80*, 113410.
19. Langer, T.; Pfnur, H.; Schumacher, H. W.; Tegenkamp, C. Graphitization process of SiC(0001) Studied by Electron Energy Loss Spectroscopy. *Appl. Phys. Lett.* **2009**, *94*, 112106–3.
20. Oida, S.; McFeely, F. R.; Hannon, J. B.; Tromp, R. M.; Copel, M.; Chen, Z.; Sun, Y.; Farmer, D. B.; Yurkas, J. Decoupling Graphene from SiC(0001) *via* Oxidation. *Phys. Rev. B* **2010**, *82*, 041411.
21. Ichikawa, Y. H. Characteristic Energy Loss of Electrons in Graphite. *Phys. Rev.* **1958**, *109*, 653–657.
22. Kresse, G.; Hafner, J. *Ab Initio* Molecular Dynamics for Liquid Metals. *Phys. Rev. B* **1993**, *47*, 558–561.
23. Kresse, G.; Furthmüller, J. Efficiency of *ab-Initio* Total Energy Calculations for Metals and Semiconductors Using a Plane-Wave Basis Set. *Comput. Mater. Sci.* **1996**, *6*, 15–50.
24. Blöchl, P. E. Projector Augmented-Wave Method. *Phys. Rev. B* **1994**, *50*, 17953–17979.
25. Kresse, G.; Joubert, D. From Ultrasoft Pseudopotentials to the Projector Augmented-Wave Method. *Phys. Rev. B* **1999**, *59*, 1758–1775.
26. Perdew, J. P.; Burke, K.; Ernzerhof, M. Generalized Gradient Approximation Made Simple. *Phys. Rev. Lett.* **1996**, *77*, 3865–3868.
27. Ehrenreich, H.; Cohen, M. H. Self-Consistent Field Approach to the Many-Electron Problem. *Phys. Rev.* **1959**, *115*, 786–790.
28. Gajdoš, M.; Hummer, K.; Kresse, G.; Furthmüller, J.; Bechstedt, F. Linear Optical Properties in the Projector-Augmented Wave Methodology. *Phys. Rev. B* **2006**, *73*, 045112.